

# Vortex structure and dynamics in kagomé and triangular pinning potentials

M. F. Laguna, C. A. Balseiro, and D. Domínguez  
*Centro Atómico Bariloche, 8400 San Carlos de Bariloche, Río Negro, Argentina*

Franco Nori

*Center for Theoretical Physics and Department of Physics, The University of Michigan, Ann Arbor, Michigan 48109-1120*  
 (Received 27 February 2001; published 20 August 2001)

We study the dynamics of thermally driven superconducting vortices in two types of periodic pinning potentials: kagomé and triangular. For the first, second, and third matching fields, we obtain the corresponding ground-state vortex configurations and their phase diagrams. We analyze the system properties by looking at the vortex trajectories and the structure factor, as well as the linear and angular diffusion. The temperature versus pinning force phase diagram is analyzed in detail for each matching field. When the temperature is varied, we observe several stages of lattice pinning and melting. In most of the cases we find, for decreasing temperature, first a pinning of vortices and afterwards a freezing transition of the interstitial vortices. The intermediate regime corresponds to interstitial vortices in a confined liquidlike state and pinned vortices. The kagomé pinning potential shows interesting behavior at low temperatures: there is a phase with rotating vortex triangles caged by kagomé hexagons (“cooperative ring elementary excitations”), and there is geometric frustration for  $T \rightarrow 0$  with a nearly degenerate ground state.

DOI: 10.1103/PhysRevB.64.104505

PACS number(s): 74.60.Ge, 74.80.-g, 74.60.Jg

## I. INTRODUCTION

Kagomé structures have been extensively used to study several physical phenomena. One refers to a central question in magnetism: the  $T=0$  order of the two-dimensional (2D) nearest-neighbor-coupled Heisenberg antiferromagnet. The kagomé lattice seems to be the first 2D spin-1/2 model with vanishing further-neighbor interactions, which appears to have a disordered ground state.<sup>1</sup> Kagomé structures have also been used to study quite different systems. For instance, measurements of the heat capacity of <sup>3</sup>He absorbed on graphite at millikelvin temperatures have been recently interpreted using a kagomé lattice structure.<sup>2</sup> In addition, measurements on the layered oxide  $\text{SrCr}_{8-x}\text{Ga}_{4+x}\text{O}_{19}$ , with kagomé-like layers, have attracted considerable attention.<sup>3</sup> The connection between the *ideal* kagomé network and the *real* structures mentioned above (e.g., <sup>3</sup>He absorbed on graphite and  $\text{SrCr}_{8-x}\text{Ga}_{4+x}\text{O}_{19}$ ) is somewhat unclear, because of the very important effects of disorder, impurities, three-dimensionality, etc., present in those materials.

It would be useful to address these and related physical questions linked to kagomé-type structures using more controllable experimental systems. One candidate for this would be to use periodic pinning arrays interacting with a vortex lattice.<sup>4–30</sup> As a function of temperature, many types of vortex arrangements appear due to the competition between the repulsive vortex-vortex interaction and the attractive vortex-pinning force.<sup>6,14–19</sup> This field is of great interest both theoretically<sup>16–30</sup> and experimentally.<sup>4–15</sup>

Superconducting networks and arrays of pinning sites (realizable, for instance, via Bitter pinning or irradiation, or made with electron-beam lithography) offer the possibility of experimentally studying nearly perfect kagomé structures. When immersed in an externally applied magnetic field, superconducting networks<sup>5,32</sup> made of thin wires, proximity-effect junctions, and tunnel junctions exhibit complex and interesting forms of phase diagrams. Kagomé structures of

this type<sup>33,34</sup> and kagomé arrays of pinning sites can be produced in a very controlled manner, and allow the possibility to study some of the unique features present in kagomé structures, like frustration, degeneracy, and metastability. Recent applications of artificial kagomé lattices even include the two-dimensional kagomé photonic bandgap waveguide.<sup>35</sup>

An important role of the behavior of the vortex system is carried out by the interstitial vortices, which produce a remarkable variety of stabilized vortex lattices that can be observed both in experiments<sup>12</sup> and simulations.<sup>17,18</sup> Commensurability in the ground-state vortex configuration enhances the pinning effect.<sup>11,12,17,18</sup> Therefore, it is very useful to determine what the matching configurations are for the different pinning geometries and, more importantly, how temperature affects them. Several geometries of arrays of pins were studied in detail by Reichhardt *et al.*,<sup>17</sup> but mostly at  $T=0$ . For instance, they obtained vortex lattice configurations for several values of the magnetic field, and they calculate the matching fields at which commensurate vortex configurations may occur. The central emphasis here will be on the effects of temperature on the vortex dynamics on two types of geometries: kagomé and triangular.

As a function of temperature, this paper (1) studies the vortex ground states obtained for a kagomé periodic array of pinning sites, (2) studies the types of multistage melting of these ground states when the temperature is slowly varied, and (3) compares these results with the simpler case of a triangular pinning potential.

In particular, for the second matching field in a kagomé lattice we find at low temperatures bistable collective states of three interstitial vortices with “cooperative ring elementary excitations” and, at  $T=0$ , degenerate ground states with geometric frustration.

## II. MODEL

We perform numerical simulations with Langevin dynamics for a two-dimensional system of vortices interacting with

a periodic pinning potential. These model the dynamics of parallel 3D rigid vortices. The dynamical equations are<sup>17</sup>

$$\eta \mathbf{v}_i = \mathbf{f}_i = \mathbf{f}_i^{vv} + \mathbf{f}_i^{vp} + \mathbf{f}_i^T, \quad (1)$$

where  $\mathbf{v}_i = d\mathbf{r}_i/dt$  is the vortex velocity,  $\eta$  is the Bardeen-Stephen friction, and

$$\mathbf{f}_i^{vv} = -\nabla U^{vv} = \sum_{j \neq i} \frac{F_v}{r_{ij}} (1 - r_{ij}^2/r_c^2) \hat{r}_{ij} \quad (2)$$

describes the vortex-vortex interaction,<sup>31</sup> which has a cutoff at a distance  $r_c$ . Here  $F_v$  is the maximum force between vortices. The sum in Eq. (2) computes the interaction between the  $i$ th vortex and all the vortices at a distance  $r_{ij} < r_c$ .

The pinning is modeled as a triangular or a kagomé array of attractive Gaussian wells with

$$\mathbf{f}_i^{vp} = -\nabla U^{vp} = -\sum_{j'=1}^{N_p} \frac{F_p}{r_p} \exp(-r_{ij'}^2/r_p^2) \hat{r}_{ij'}, \quad (3)$$

where  $F_p$  is the maximum pinning force,  $r_p$  is the radius of the pinning site, and  $r_{ij'}$  is the distance between the vortex  $i$  and the pinning site  $j'$ . The sum in Eq. (3) is over the  $N_p$  pinning sites.

The effect of temperature is added as a stochastic term with properties

$$\langle f_i^T(t) \rangle = 0 \quad (4)$$

and

$$\langle f_i^T(t) f_j^T(t') \rangle = 2 \eta k_B T \delta(t-t') \delta_{ij}. \quad (5)$$

We measure all lengths in units of  $r_c$ , the range of the vortex-vortex interaction, and all the forces in units of  $F_v$ . Here, the pinning radius  $r_p$  was varied from 0.05 to 0.1, and the pinning sites can trap only one vortex. We consider pinning forces  $F_p$  varying from 0 to 5, but in some cases, we increase the pinning intensity up to very large values, like  $F_p = 50$ . The number of vortices varies from 16 to 4096. We use periodic boundary conditions in all cases shown here. Depending on the particular simulation, the time step  $\Delta t$  was chosen in the interval  $[0.01, 0.0001]$ , with the number of simulations steps varying in the interval  $[10^4, 10^8]$ .

We define the  $n$ th matching field (MF) as the magnetic field that generates a number of vortices  $N_v$  which is an integer multiple of the number of pinning sites of a triangular lattice,  $N_p^t$ :

$$N_v/N_p^t = n. \quad (6)$$

Thus, for the triangular pinning case the number of interstitial vortices is

$$N_i^t = N_v - N_p^t = (n-1)N_p^t. \quad (7)$$

There is a relationship between the number of sites of the triangular and kagomé lattices,

$$N_p^k = (3/4)N_p^t, \quad (8)$$

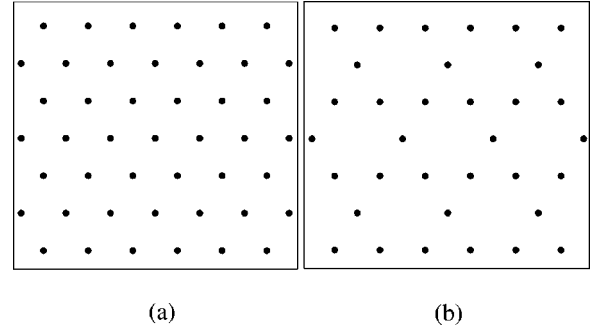


FIG. 1. (a) Triangular lattice. (b) Kagomé lattice. Note that this lattice can be constructed with hexagonal cages (*kagomé hexagons*) and triangles pointing up and down (*kagomé triangles*).

where  $N_p^k$  is the number of pinning sites of the kagomé lattice (see Fig. 1). Then, for the  $n$ th MF  $N_v/N_p^k = 4n/3$ . The number of interstitial vortices in the kagomé pinning case is

$$N_i^k = N_v - N_p^k = (4n/3 - 1)N_p^k = (n - 3/4)N_p^t. \quad (9)$$

It is important to notice that the fraction of interstitial vortices  $N_i^k/N_v = 1 - 3/(4n)$  and  $N_i^t/N_v = 1 - 1/n$  varies significantly for the different MF's. For the first MF,  $N_i^k/N_v = 1/4$  and  $N_i^t/N_v = 0$  (there are no interstitial vortices present in the triangular case); for the second MF,  $N_i^k/N_v = 5/8$  and  $N_i^t/N_v = 1/2$ ; and for third MF,  $N_i^k/N_v = 3/4$  and  $N_i^t/N_v = 2/3$ .

The vortex density corresponds to 2.5 vortices per unit length and it is a constant for all the MF studied here. Consequently the pinning density varies with the different MF. For the first MF's it is the same as the vortex density, and is lower for higher MF's. We have examined the vortex lattice ordering up to the fourth MF (although we will describe here only the first three MF's).

### III. CALCULATED QUANTITIES

#### A. Ground states and trajectories

To find the vortex ground state, we gradually cool down a fixed number of randomly moving vortices from a high temperature to  $T=0$ . A useful picture of the way in which the vortices go from the liquid to the solid phase is provided by the vortex trajectories for a fixed temperature. When the system is at high enough temperatures, the vortices move quickly and their trajectories occupy all the space. Some of them occasionally go inside a pinning site, spend some time there, and then get out of the local potential trap. This general trend was observed for all of the MF's studied when the temperature  $T > T_p$ , with  $T_p$  the pinning temperature.

At  $T < T_p$ , a subset of  $N_p$  vortices are trapped in the  $N_p$  pinning sites. These vortices move inside the potential well, but they do not have enough energy to go out of their pinning site. The remaining  $N_i$  interstitial vortices, however, are free to move, and they describe trajectories which depend on the MF studied. The behavior of the vortex system in the cooling down process as well as the characteristic final state will be explained in detail for each MF.

### B. Diffusion

To quantify the motion of the vortices, we calculate their linear diffusion  $D$  as the coefficient of the mean-squared displacements  $\langle \Delta r^2 \rangle$  at long times:

$$\langle \Delta r^2 \rangle = \frac{1}{N} \left\langle \sum_{i=1}^N |\mathbf{r}_i(t) - \mathbf{r}_i(0)|^2 \right\rangle \propto D t, \quad (t \rightarrow \infty). \quad (10)$$

The diffusion can be seen more clearly if we plot directly the  $\langle \Delta r^2 \rangle$  at different time scales as a function of temperature. For high temperatures, when the vortices have essentially unbounded motion, the  $\langle \Delta r^2 \rangle$  is linear with time. For low temperatures, the displacements are time independent and smaller than  $a$ , the average distance between vortices. We find that this change of behavior occurs at a temperature  $T_i$ , the freezing temperature of interstitial vortices. In other words,  $T_i$  is a signature of “bounded vortex motion” and can be directly measured from the  $\langle \Delta r^2 \rangle$ .

In order to study the vortex motion, we can follow the individual squared displacement of each vortex,

$$\Delta r^2(i) = |\mathbf{r}_i(t) - \mathbf{r}_i(0)|^2, \quad (11)$$

which allows us to distinguish the behavior of pinned and interstitial vortices. Thus, it is useful to define the following quantities:  $T_p$  as the temperature below which the  $\Delta r^2$  of a pinned vortex is lower than  $r_p^2$ , the squared pinning radius, and  $T_i$  as the temperature below which the interstitial vortices have  $\Delta r^2 < a^2$ .

Another way to study the vortex diffusion is by monitoring a combination of  $\langle \Delta r^2 \rangle$  and  $\Delta r^2(i)$ , defined as  $\langle \Delta r^2(v) \rangle$ , where  $v = p, i$ , depending on the kind of vortex studied (pinned or interstitial). Thus, for instance,

$$\langle \Delta r^2(p) \rangle = \frac{1}{N_p} \left\langle \sum_{i=1}^{N_p} |\mathbf{r}_i(t) - \mathbf{r}_i(0)|^2 \right\rangle,$$

where the sum is over the vortices that are pinned for temperatures lower than  $T_p$ .

### C. Pinned fraction

We define the pinned fraction  $\chi$  as the fraction of the total number of vortices,  $N_v$ , with displacements lower than  $r_p$ :

$$\chi(T) = N(T)/N_v, \quad (12)$$

where  $N(T)$  is the number of vortices with  $\Delta r^2(i) < r_p^2$  at the temperature  $T$ . In the solid vortex phase  $\chi = 1$ , and in the liquid phase  $\chi \approx 0$ . In the intermediate region, where the interstitial vortices move while the others are pinned,  $\chi = N_p^t/N_v = 1/n$  for the triangular lattice, whereas  $\chi = N_p^k/N_v = 3/4n$  for the kagomé lattice. If the solid-liquid phase transition is direct,  $\chi$  will change discontinuously from 0 to 1 in the thermodynamic limit, without any indication of an intermediate region. As we show below, the behavior of this quantity is a very good indicator of  $T_p$  and  $T_i$ .

### D. Structure factor

In order to analyze the structural order of the vortex array in the different phases, we calculate the structure factor of the vortex system at each temperature as

$$S(\mathbf{k}) = \frac{1}{N^2} \left\langle \left| \sum_j e^{i\mathbf{k} \cdot \mathbf{r}_j} \right|^2 \right\rangle. \quad (13)$$

In the liquid phase  $S(\mathbf{k}) \propto 1/N^2$ , whereas in the solid phase  $S(\mathbf{k}) \approx 1$ . We studied the behavior of two peaks of the structure factor, one corresponding to a wave vector  $\mathbf{k} = (2\pi/a, 0)$  of the triangular lattice of vortices and the other with  $\mathbf{k} = (3\pi/2a, \sqrt{3}\pi/2a)$  which belongs to the kagomé lattice of the pinning sites. We analyze the behavior of the height of those peaks as a function of temperature for the different MF's. They have a maximum in the regions in which the vortex structure has the geometry of the lattice that they represent.

## IV. PHASE DIAGRAMS

We start by presenting an overview of the phase diagrams of *temperature versus pinning strength* for both the triangular and kagomé lattices. These diagrams were obtained by analyzing the temperature dependence for the quantities described in the previous sections. The details of how the phase boundaries were obtained are described in the following sections.

The phase diagram for the first MF is shown in Fig. 2 and is qualitatively the same for the triangular [Fig. 2(a)] and kagomé [Fig. 2(b)] pinning geometries. For the range of pinning strengths studied here, we find one characteristic temperature  $T_p$ , above which the vortex system is in a *liquid phase* with all the vortices moving through the sample. For temperatures lower than  $T_p$  all vortices are localized around their equilibrium positions and the system is in a *solid phase*.

The temperature  $T_p$  grows with the strength of the pinning potential, which is characterized by the maximum pinning force  $F_p$ . We find that  $T_p(F_p)$  is slightly higher for the triangular pinning potential than for the kagomé one. This is because, for the first MF, in the triangular lattice every vortex can be trapped at a pinning site, whereas in the kagomé case about 1/4 of the vortices are not core pinned—namely, 25% of the total number  $N_v$  of vortices have their equilibrium positions inside the hexagonal kagomé cages (*kagomé hexagons*). The  $N_i^k$  interstitial vortices vibrate more than the pinned ones, lowering the freezing temperature.

For the kagomé pinning case, we have checked the behavior of the vortex system up to extremely large values of the pinning force, up to  $F_p = 50$  (10 times the higher  $F_p$  showed in the phase diagram). We find only one freezing temperature  $T_p$ , until reaching some pinning intensity, above which the vortex motion is dominated by the pinning force. In that limit, the vortex system has a different evolution with temperature which is not studied in the present work. In other words, in the parameter range studied in this paper, we find only one freezing temperature  $T_p$ . When the pinning force becomes very large compared with the vortex-vortex repulsion force, the problem becomes different and beyond the

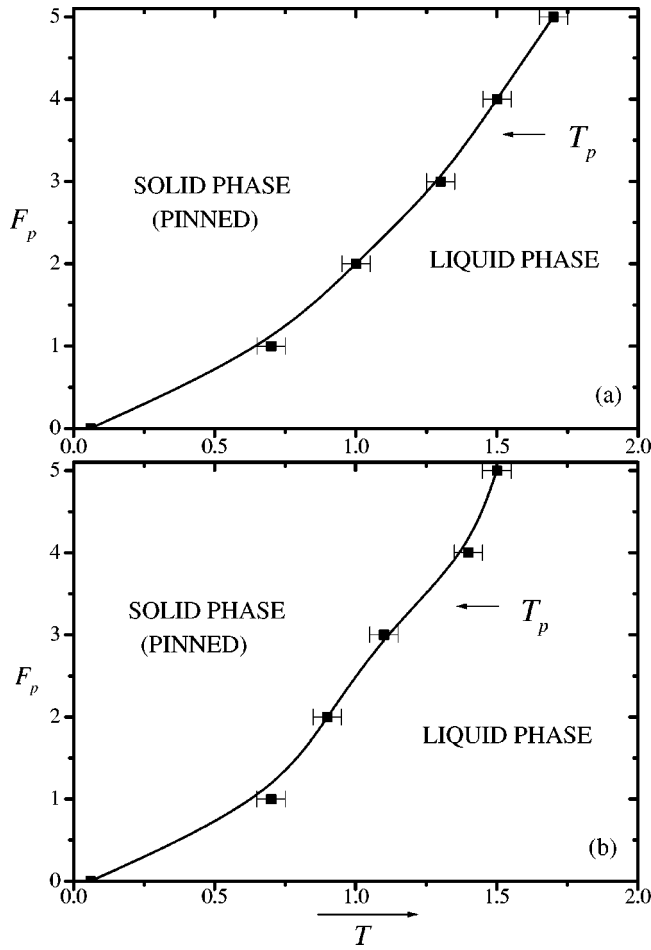


FIG. 2. Phase diagram  $T$ - $F_p$  of temperature vs pinning force strength for the first MF. The pinning potentials form triangular (a) and kagomé (b) lattices. In all the figures, including this one, the temperature scale is multiplied by a factor of  $10^3$ .

scope of this paper. Here we are interested in the interplay of attractive (pinning) forces, repulsive (vortex-vortex) forces, and disordering (thermal) forces.

For the first MF, we could not find a temperature range in which two separated characteristic temperatures appear. It is possible that the short distance between the pinned vortices in the first MF (due to the high pinning density) makes impossible the crossing of the interstitial vortices between two pinning sites. If that is the case, the only allowed movements are the oscillation inside a kagomé hexagon and the creeplike motion of all the vortices among the pinning sites. As we will see below,  $T_i$  (the interstitial freezing temperature of  $N_i^t$  vortices) appears for MF's higher than 1, where we can access an intermediate phase in which some vortices are pinned and other are in a liquidlike state.

The second MF has the most interesting behavior as a function of temperature. The vortex dynamics in this case is different for the two pinning geometries studied, as we can observe in Fig. 3. This is the only MF studied that does not have a triangular ground state for the two pinning geometries used. Indeed, Figs. 9(d) and 11(d) show this. The triangular pinning case has been studied in some detail<sup>17</sup> and at low temperatures vortices form a honeycomb structure [Fig.

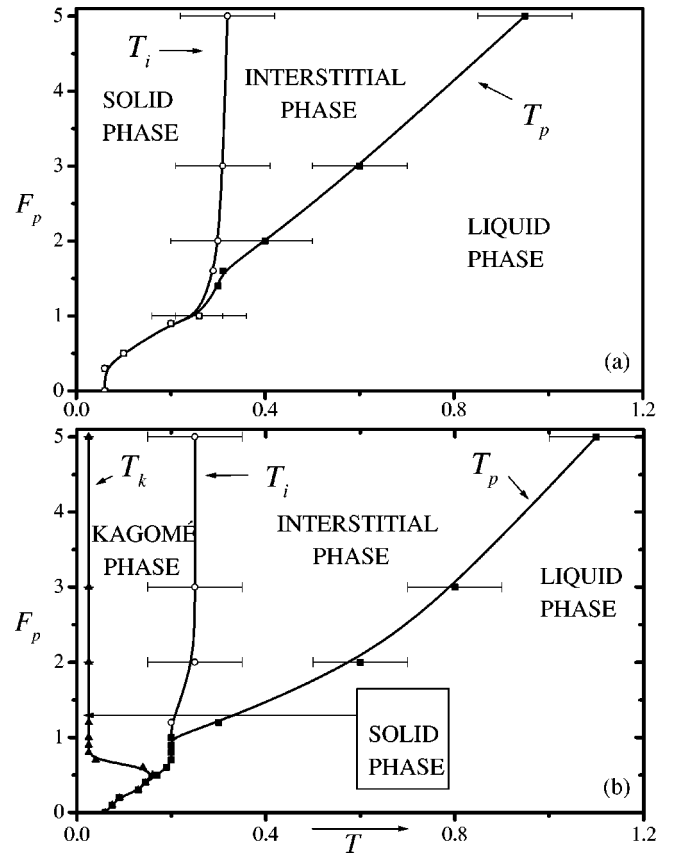


FIG. 3. Phase diagram  $T$ - $F_p$  of temperature vs pinning force strength for the *second* MF. The pinning potentials form triangular (a) and kagomé (b) lattices.

9(d)]. For high pinning forces ( $F_p > 1$ ) the phase diagram shows two relevant temperatures  $T_p$  and  $T_i$  [Fig. 3(a)]. The first one is the pinning temperature, below which  $N_p^t$  vortices are trapped by the  $N_p^t$  pinning sites. The  $N_i^t$  remaining vortices move freely. At a lower temperature  $T_i$  they freeze and the system is in the *solid phase*. The intermediate region of temperatures, in which some vortices are pinned and others are moving, is the “melted interstitial vortex phase” or *interstitial phase*, for short.  $T_p$  grows with  $F_p$  because the transition between these two phases depends on the vortex-pinning interaction. On the other hand,  $T_i$  mostly depends on the vortex-vortex interaction; consequently, it is almost  $F_p$  independent. For a finite pinning intensity  $F_p \approx 1$ , the two transitions merge in a single one ( $T_i = T_p$ ) and the interstitial phase disappears. For  $F_p < 1$  the system has a single solid-liquid transition and the ground state changes from the honeycomb to the triangular lattice, which is the ground state of the vortex system without pinning potential. These results will be presented elsewhere.

The kagomé pinning geometry [Fig. 3(b)] generates a *kagomé phase*, an intermediate phase which is neither a solid phase nor the interstitial phase that appears at a higher temperature. This case has three characteristic temperatures  $T_p$ ,  $T_i$ , and  $T_k$ . The pinning temperature  $T_p$  has the same features as in the previous case, and its behavior as a function of  $F_p$  is similar to the triangular pinning case. At the tempera-

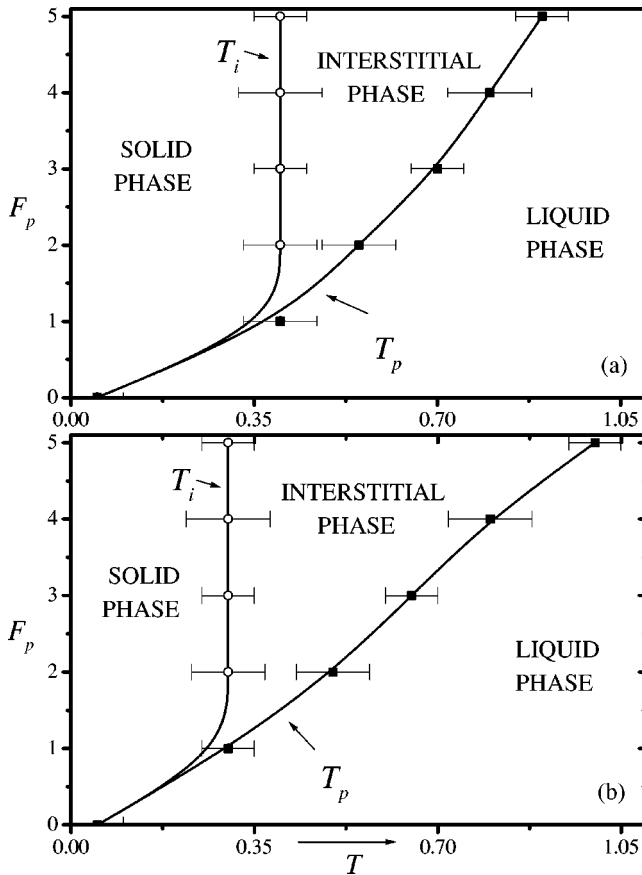


FIG. 4. Phase diagram  $T$ - $F_p$  of temperature vs pinning force strength for the *third* MF. The pinning potentials form triangular (a) and kagomé (b) lattices.

ture  $T_i$ , a fraction of interstitial vortices (which are localized inside the kagomé triangles) freeze, but the vortices trapped in the kagomé hexagons are still moving. The behavior of the three vortices trapped in each hexagon is very particular. They form triangles which can rotate over a bistable configuration. Indeed, in this temperature regime the ground state is highly degenerate, because each vortex triangle can have two possible orientations. Certainly, these vortex triangles move until very low temperatures are reached, and only at  $T = T_k$  do they freeze and the vortex system enter the solid phase. These triangles form a frustrated triangular lattice. The kagomé phase has an approximately constant width in the range  $1 < F_p < 5$ . This phase and the interstitial phase both disappear for  $F_p \lesssim 1$  (indeed,  $T_i = T_p$  for  $F_p \approx 1$ ). In the low-pinning region  $F_p < 1$ , the vortex system goes directly from the liquid high-temperature phase to the solid phase, and the ground state changes from the disordered glassy state to the triangular lattice (at  $F_p = 0$ ) passing through several structures, which are combinations of triangular, squared, and kagomé structures. The case of weak pinning ( $F_p < 1$ ) will be studied in a future work.

Finally, the third MF has the phase diagram shown in Fig. 4. The behavior of the vortex system for the two pinning geometries is very similar, with two relevant temperatures  $T_p$  and  $T_i$  defined as in the previous cases. The phase diagram has a behavior which is similar to the case of the second MF

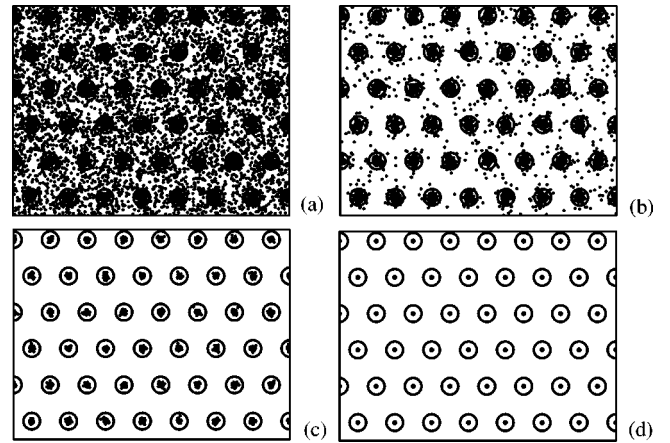


FIG. 5. Vortex trajectories for the first MF of vortices in a triangular pinning lattice. (a)  $T > T_p$ , liquid phase. (b)  $T \approx T_p$ . (c)  $T < T_p$ , solid phase. (d)  $T = 0$ , ground state.

for the triangular pinning lattice. Although this MF has a triangular ground state (as the first MF), the interstitial phase is present at every pinning intensity higher than  $F_p = 1$ .

In what follows, we will analyze in some detail the physical quantities that are used to characterize the different phases and phase boundaries.

## V. FIRST MATCHING FIELD

In this section we describe the results for a vortex system with  $N_v/N_p^t = 1$ . We first show the results for the triangular pinning lattice, which are simpler to understand. Then, we compare these results with the corresponding ones obtained for the kagomé pinning lattice.

### A. Triangular pinning potential

In Figs. 5(a)–5(d) we show the vortex trajectories for different temperatures in the cooling down process for the first MF. In this case, every vortex has a pinning site where it can be trapped. In Fig. 5(a) the system is at a high temperature  $T > T_p$ , and the vortex system behaves as a liquid only slightly perturbed by the pinning structure. At  $T \approx T_p$  [Fig. 5(b)] all vortices become trapped in the pinning sites. At  $T < T_p$  the system is in a solid phase. The pinned vortices are vibrating but they do not go out of their pinning sites. This situation can be observed in Fig. 5(c).

Finally, by cooling the vortex system until  $T = 0$  we find a triangular ground state.<sup>17</sup>

The behavior of the fraction  $\chi$  of pinned vortices is a good indicator of a single solid-liquid transition in the first MF. At high temperatures,  $\chi = 0$ , indicating that all vortices are depinned. At low temperatures,  $\chi = 1$ , characteristic of a solid phase with no interstitial vortices. There is a characteristic temperature  $T_p$  around which  $\chi$  rapidly changes from 0 to 1, as can be seen in Fig. 6(a). As we show below, this way of defining the pinning temperature  $T_p$  coincides with the  $T_p$  obtained by analyzing other quantities like diffusion constants or structure factor. Thus, we have verified the consistency of the criteria used to define phase boundaries.

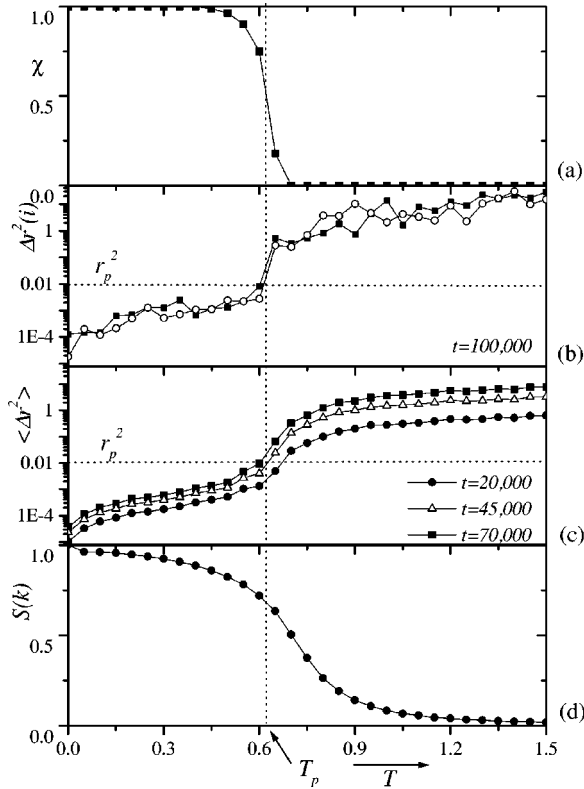


FIG. 6. First MF of 1024 vortices and  $F_p=1$ . All the panels here correspond to the triangular lattice of pinning traps. The following quantities were calculated vs temperature: (a) Pinned fraction. (b)  $\Delta r^2(i)$  of two pinned vortex (there are no interstitial vortices in this case). (c)  $\langle \Delta r^2 \rangle$  at different time scales. (d) Height of the peak of the structure factor corresponding to the triangular lattice of vortices.

The squared displacement of individual vortices  $\Delta r^2(i)$  versus  $T$  at a fixed time ( $t=100\,000$ ) for a system of 1024 vortices and  $F_p=1$  is shown in Fig. 6(b) for two different vortices. For all vortices  $\Delta r^2$  has a jump at the same temperature  $T_p$ , with  $\Delta r^2 > r_p^2$  for  $T > T_p$  and  $\Delta r^2 < r_p^2$  for  $T < T_p$ .

The mean-squared displacement  $\langle \Delta r^2 \rangle$  (an average of the individual squared displacements) as a function of temperature at different time scales is shown in Fig. 6(c) for the same parameters than Fig. 6(b). At different time scales, the general behavior of  $\langle \Delta r^2 \rangle$  is the same, showing a rapid variation around  $T_p$ . For  $T > T_p$  we find  $\langle \Delta r^2 \rangle > r_p^2$  and its value depends on the time scale. A detailed analysis shows a linear dependence of  $\langle \Delta r^2 \rangle$  with time, characteristic of a diffusive process (note the logarithmic scale in the figure). For  $T < T_p$  we find  $\langle \Delta r^2 \rangle < r_p^2$  for all time scales.

Finally, we studied the intensity of the triangular peak  $k=(2\pi/a,0)$  of the structure factor. The behavior of that peak height as a function of temperature is showed in Fig. 6(d), and has its maximum height at  $T=0$ , when the triangular vortex lattice is perfectly ordered. As the temperature increases, the triangular peak decreases and at high temperatures is proportional to  $1/N_p^2$ . Note that although the structure factor is consistent with the behavior of the other quantities, it is not a good indicator of the phase transition since it has important finite size effects.

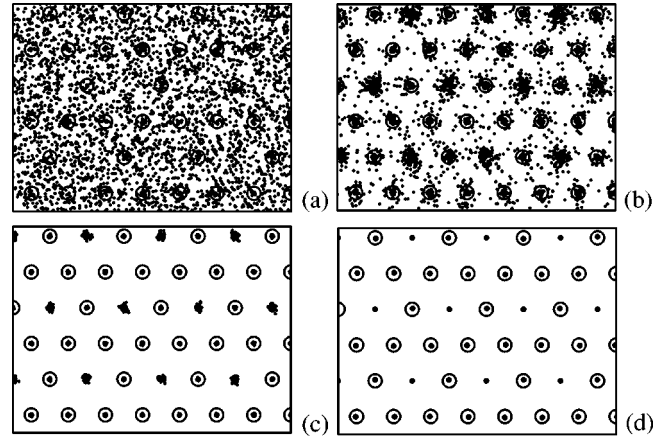


FIG. 7. Vortex trajectories of vortices, for the first MF, on a kagomé pinning geometry. (a)  $T > T_p$ , liquid phase. (b)  $T = T_p$ . (c)  $T < T_p$ , solid phase. (d)  $T=0$ , ground state.

Following this procedure for each pinning force we were able to define with good precision the transition temperature  $T_p$  and build the phase diagram of Fig. 2(a).

## B. Kagomé pinning potential

The behavior of the vortex system for the first MF with a kagomé lattice pinning is very similar to the previous case.

By following the vortex trajectories it is clear that at high temperatures the system is in a liquid state, as seen in Fig. 7(a). As the temperature is lowered, a number  $N_p^k$  of vortices become trapped in the  $N_p^k$  pinning sites, as can be seen in Fig. 7(b). As we show below, when the  $N_p^k$  vortices are trapped in the pinning centers, the  $N - N_p^k$  interstitial vortices are trapped in the kagomé hexagons, and there is a single transition from the liquid to the solid phase. The solid phase is shown in Figs. 7(c) and 7(d).

Finally, at  $T=0$ , we find the ground state for the first MF [Fig. 7(d)]. The vortex lattice is triangular, highly ordered, and the same as for the case for a triangular pinning lattice.<sup>17</sup> The vortices occupy every pinning site, no matter how weak the vortex-pinning interaction is. For the first MF (and also for the fourth MF) the triangular vortex lattice is nonrotated with respect to the pinning array and it is stable under small perturbations.

The pinned fraction  $\chi$  has the same behavior as in the triangular pinning case. For all the  $F_p$  studied we find the same kind of curve as we show in Fig. 8(a). Thus, the general trend is robust. There is no indication of two relevant temperatures, as we see clearly for the other MF's (see below). The temperature  $T_p$  is defined as the temperature at which  $\chi=0.5$ , and it increases with  $F_p$ .

We plot  $\Delta r^2(i)$  versus  $T$  at  $t=100\,000$  in Fig. 8(b). By following two vortices, one that is pinned and the other that is occupying an interstitial position at  $T=0$ , we find that both have a jump in  $\Delta r^2$  at the same temperature  $T_p$ . The interstitial vortex has  $\Delta r^2(i) < a^2$  for  $T < T_p$ , whereas the pinned vortex has  $\Delta r^2(p) < r_p^2$  for  $T < T_p$ , in agreement with what we saw in the trajectories of Fig. 7.

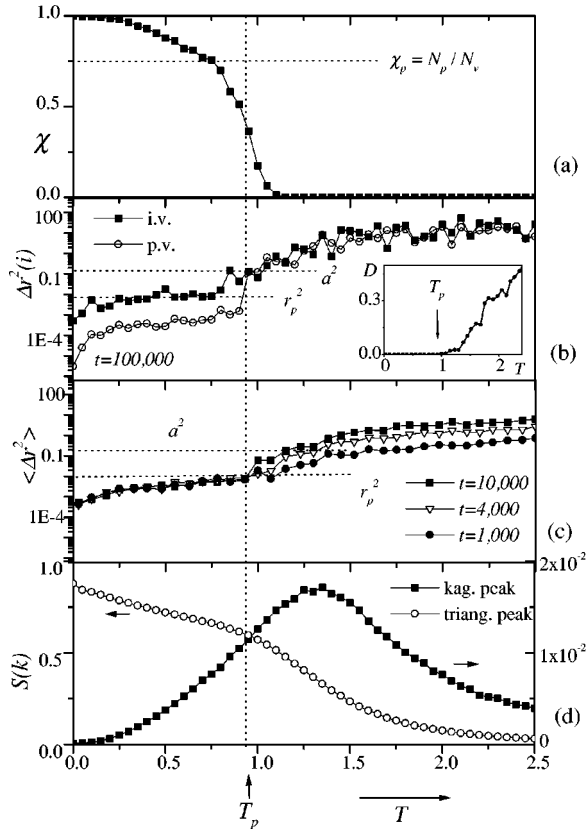


FIG. 8. First MF of 1024 vortices and  $F_p = 3$ . The plots here are for the kagomé pinning lattice. The following quantities were calculated vs temperature: (a) Pinned fraction. (b)  $\Delta r^2(i)$  of a pinned vortex (open symbols) and a interstitial vortex (solid symbols). Inset: Linear diffusion coefficient  $D$  vs temperature. (c)  $\langle \Delta r^2 \rangle$  at different time scales. (d) Height of two peaks of the structure factor. One corresponding to the triangular lattice of vortices (open symbols) and the other to the kagomé pinning lattice (solid symbols).

In Fig. 8(c) we show the  $\langle \Delta r^2 \rangle$  as a function of temperature at different time scales for the same parameters as Fig. 8(b). We observe that for  $T > T_p$  the  $\langle \Delta r^2 \rangle$  are linear with time, while for  $T < T_p$  the displacements are independent of time and lower than the square of the characteristic lengths  $a$  and  $r_p$ . We also obtained the linear diffusion coefficient  $D$  versus  $T$  and found that for  $T < T_p$  the diffusion coefficient is  $D \approx 0$ , and at  $T = T_p$  it starts to grow [see the inset of Fig. 8(b)].

Finally, we show in Fig. 8(d) the intensity of two peaks of the structure factor, one for the triangular vortex lattice [ $k = (2\pi/a, 0)$ ] and the other belonging to the kagomé lattice of pinning sites [ $k = (3\pi/2a, \sqrt{3}\pi/2a)$ ], both as a function of temperature. We observe that the triangular peak has its maximum height at  $T = 0$ , with a similar behavior as the peak of the triangular pinning case. However, the kagomé peak has a small maximum at a temperature  $T \approx T_p$  at which vortices are not pinned but they spend a long time at the pinning centers, forming a kagomé lattice. The fast movement of vortices in the interstitial space disguises the triangular structure.

All these results summarized in Fig. 2(b) indicate a single transition between a high-temperature liquid phase, in which

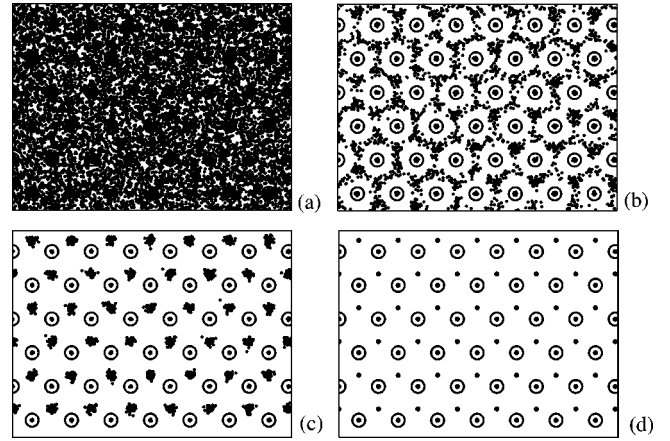


FIG. 9. Vortex trajectories for the second MF with a triangular pinning potential. (a)  $T > T_p$ , liquid phase. (b)  $T_i < T < T_p$ , interstitial phase. (c)  $T < T_i$ , solid phase. (d)  $T = 0$ , final state.

all vortices diffuse, to a low-temperature solid phase in which all vortices are pinned, despite the fact that only 75% of the vortices are trapped in pinning sites. The pinning temperature  $T_p$  increases with the pinning intensity  $F_p$  and it is slightly lower than the transition temperature for a vortex system in a triangular pinning lattice.

## VI. SECOND MATCHING FIELD

In this section we describe the results for a vortex system with  $N_v/N_p^t = 2$ . The behaviors of the system with triangular and kagomé pinning lattices are very different and they will be described in the next two subsections.

### A. Triangular pinning potential

The trajectories followed by the vortices from high to low temperatures are shown in Fig. 9. The region  $T > T_p$  is a liquid [Fig. 9(a)]. At  $T < T_p$  there are  $N_p^t$  vortices pinned. In the interstitial region [see Fig. 9(b)]  $T_i < T < T_p$  the  $N_v - N_p^t$  interstitial vortices move freely and finally they freeze at  $T_i$  [Fig. 9(c)]. The ground state is shown in Fig. 9(d). The vortex structure at  $T = 0$  is a honeycomb lattice, with some defects, and it has two possible ground states, which were studied in Ref. 17. In that work the authors show that this structure disappears for weak pinning because the ordering is not met by commensurability effects but by the dominance of the pinning force. Also, these authors looked at the magnetization and critical current versus field.

We did the same kind of analysis as for the first MF (see Fig. 10), and we find two characteristic temperatures:  $T_p$ , the pinning temperature, which is  $F_p$  dependent, and  $T_i$ , the freezing temperature of the interstitial vortices, below which the system behaves as a solid. This last temperature is almost independent of  $F_p$  for  $F_p > 1$ .

In Fig. 10(a) we plot the pinned fraction  $\chi$ , which shows that in a finite region of temperatures (between  $T_i$  and  $T_p$ ) there are exactly  $N_p^t$  vortices with  $\Delta r^2 < r_p^2$ . We find that for lower  $F_p$  the width of that region is smaller, and for  $F_p = 1$  it disappears ( $T_p$  becomes equal to  $T_i$ ).

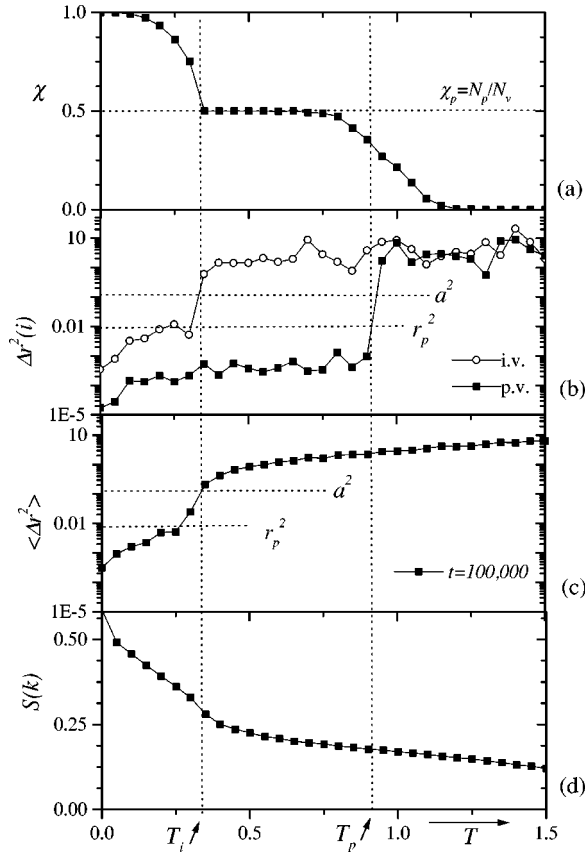


FIG. 10. Second MF of 2048 vortices and  $F_p = 5$  with triangular pinning potential. (a) Order parameter. (b)  $\Delta r^2(i)$  of a pinned vortex (solid symbols) and an interstitial vortex (open symbols). (c)  $\langle \Delta r^2 \rangle$  at  $t = 100\,000$ . (d) Triangular peak of the structure factor.

In Fig. 10(b) we can see the individual squared displacements that show a jump at two very different temperatures. The jump in the  $\Delta r^2$  of the pinned vortex is at a temperature  $T_p$ , and for  $T < T_p$  it is  $\Delta r^2 < r_p^2$ . The jump in  $\Delta r^2$  for the interstitial vortex is at a lower temperature  $T_i$  and for  $T < T_i$  it is  $\Delta r^2 < a^2$ . The mean-squared displacement  $\langle \Delta r^2 \rangle$  at  $t = 100\,000$ , shown in Fig. 10(c), has a jump at  $T_i$  but is not sensitive to  $T_p$ .

Finally, the triangular peak of the structure factor is shown in Fig. 10(d). We find that this last quantity is not sensitive to  $T_p$  for this MF.

The results of  $\chi$  and  $\Delta r^2$  [Figs. 10(a) and 10(b)] clearly show the existence of two characteristic temperatures that merge to a single one as  $F_p$  approaches 1. The other quantities ( $\langle \Delta r^2 \rangle$ , structure factor, and specific heat (not shown here)) show a change (the first two) or a maximum (the last one) at the transitions, but have important finite size effects.

### B. Kagomé pinning potential

In Fig. 11 we plot the vortex trajectories for four temperatures. Figure 11(a) corresponds to a high temperature ( $T > T_p$ ) and the system is in the liquid phase. In Fig. 11(b) the system is in the interstitial phase ( $T_i < T < T_p$ ) and we can distinguish two kinds of vortices: the ones which are pinned in the kagomé pinning sites and the others that are moving

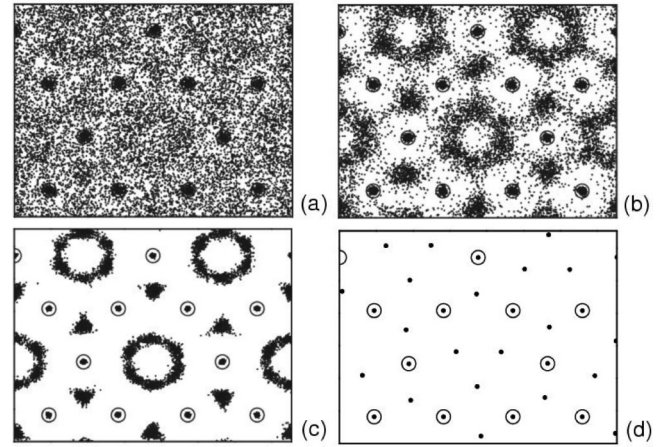


FIG. 11. Vortex trajectories for the second MF. Kagomé pinning potential. (a)  $T > T_p$ , liquid phase. (b)  $T_i < T < T_p$ , interstitial phase. (c)  $T_k < T < T_i$ , kagomé phase. (d)  $T = 0$ , ground state.

freely. At a lower temperature  $T_k < T < T_i$  we find an interesting behavior in the vortex trajectories [Fig. 11(c)]. Some of the interstitial vortices are now trapped inside the kagomé triangles (interstitial “confined freezing”), but others are moving in a circle inside the kagomé hexagons. We will see that in this regime of temperature the vortex system has angular diffusion but does not have linear diffusion. The vortices which are moving in circles (the *kagomé vortices*) form a triangle which is only slightly deformed during the rotation. At a finite temperature  $T_k$  the kagomé vortices freeze and the system is in a solid phase [Fig. 11(d)]. The second MF has a ground state which is different than the one obtained in a triangular pinning array.<sup>17</sup> For the kagomé case, the ground state is nearly degenerate because the kagomé triangles have two equivalent orientations [in Fig. 11(d) kagomé triangles can point up or down] and the perfect order is frustrated.

To find the relevant temperatures as a function of  $F_p$  we did the same analysis as the previous cases.

In Fig. 12(a) we show the pinned fraction versus temperature for  $F_p = 5$ . We define  $T_p$  as the temperature below which a finite fraction of vortices have  $\Delta r^2 < r_p^2$ . For  $F_p = 5$  this happens at a higher temperature than for  $F_p = 1$  (not shown here) and we observe a finite region of temperatures for which  $\chi = \chi_p$  ( $\chi_p = N_p^k / N_v$  is the fraction of pinning sites).

The temperature  $T_i$  is the temperature at which the interstitial vortex of Fig. 12(b) has  $\Delta r^2 \approx a^2$ . The  $T_p$  observed in Fig. 12(a) is the same as the one observed in Fig. 12(b), in which the pinned vortex has  $\Delta r^2 \approx r_p^2$ .

In Fig. 12(c) we plot the mean-squared displacements  $\langle \Delta r^2 \rangle$  for different time scales, and we can see that is  $\langle \Delta r^2 \rangle \approx a^2$  at  $T_i$ .

Finally, the two peaks of the structure factor are studied in Fig. 12(d). The triangular peak, with  $k = (\pi/a, \sqrt{3}\pi/a)$  (open symbols), has a maximum in  $T = 0$ , but this value is not 1 (as we expect for a perfect triangular vortex lattice) but  $1/3$ . This is in agreement with the ground state not being triangular [Fig. 4(d)]. The kagomé peak has a maximum at  $T \approx T_p$ , the temperature at which the kagomé vortex lattice is formed on the pinning sites.

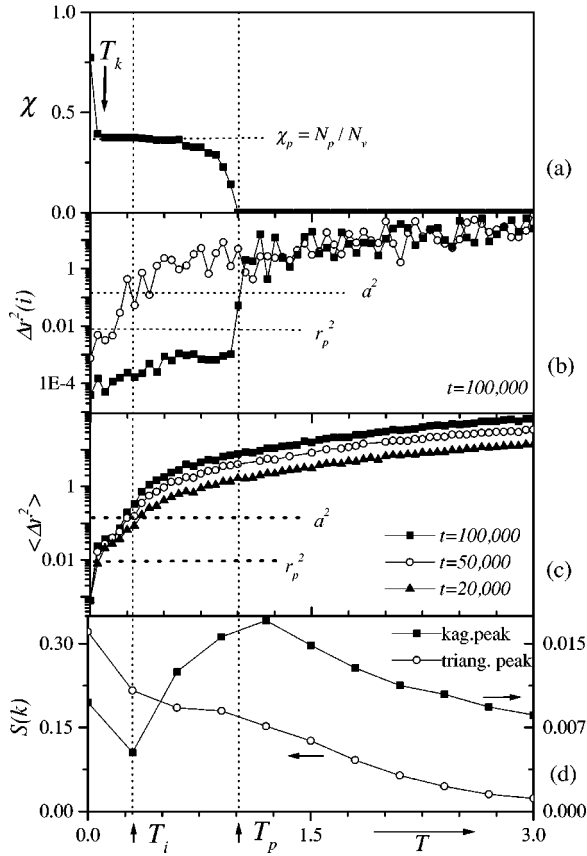


FIG. 12. Second MF of 2048 vortices and  $F_p=5$ . Quantities calculated vs temperature: (a) pinned fraction, (b)  $\Delta r^2(i)$  of a pinned vortex (solid symbols) and an interstitial vortex (open symbols); (c)  $\langle \Delta r^2 \rangle$  at different time scales, and (d) the height of two peaks of the structure factor: one corresponding to the triangular lattice of vortices (solid symbols) and the other to the kagomé pinning lattice (open symbols).

To separate the contribution to the diffusion of rotating vortices in the second MF, we calculate, for temperatures  $T < T_i$ , the mean-squared angular displacements of the vortex triangles,

$$\langle \Delta \theta^2 \rangle = \langle |\theta_i(t) - \theta_i(0)|^2 \rangle, \quad (14)$$

where  $\theta(i)$  is the average angular coordinate of the  $i$ th triangle. When  $\langle \Delta \theta^2 \rangle \leq \pi/3$  the rotation stops and the temperature at which the vortex triangles freeze is  $T_k$ .

To study the low-temperature region ( $T < T_i$ ) we calculated the same diffusive quantities than before, but we add the calculation of the  $\langle \Delta \theta^2 \rangle$ . We find that the kagomé vortices generate a finite angular diffusion for temperatures  $T_k < T < T_i$ , because  $\langle \Delta \theta^2 \rangle > \pi/3$  in this region. For  $T < T_k$  the vortex triangles oscillate around their final position but they do not change the orientation of the triangle. There is no linear diffusion because  $\langle \Delta r^2 \rangle$ ,  $\langle \Delta r^2(v) \rangle$ , and  $\Delta r^2(i)$  are lower than  $a^2$  in this range of temperature (they are moving less than the average distance between them). In Fig. 13 we show these quantities and the way in which we determine  $T_k$ .

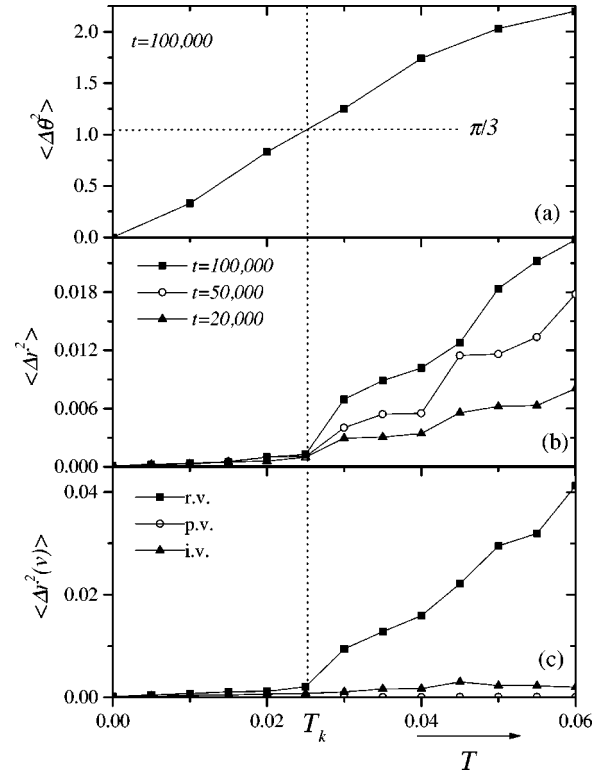


FIG. 13. Second MF of 2048 vortices and  $F_p=5$  in a kagomé pinning potential. The following quantities were calculated vs temperature for  $T < T_i$ : (a) mean-squared angular displacements of vortex triangles, (b)  $\langle \Delta r^2 \rangle$  at different time scales, and (c)  $\langle \Delta r^2(v) \rangle$  of rotating kagomé vortices (square solid symbols) pinned vortices (open symbols) and interstitial vortices (triangular solid symbols).

The region of temperatures  $T_k < T < T_p$ , for which  $\chi = \chi_p$ , corresponds to both the interstitial and kagomé phases. In both phases there are exactly  $N_p$  pinned vortices. We find that for  $F_p=1$ , then  $T_p=T_i$  (not shown here).  $T_p$  grows as  $F_p$  is increased but  $T_i$  and  $T_k$  are independent of the pinning intensity. Therefore, the widths of the kagomé and the solid phases are almost constant with  $F_p$ , but the interstitial phase (bounded by  $T_i$  and  $T_p$ ) is wider for higher  $F_p$ .

### C. Correlated ring elementary excitations

As we have seen, the second matching field in a kagomé lattice is special because it is highly degenerate. Namely, many different configurations have the same energy. While the entropy of most matching field configurations is zero for standard lattices, it is quite large for the second matching field in a kagomé lattice.

The second matching field in a kagomé lattice exhibits (i) bistable collective states of three interstitial vortices (which can be denoted  $u$  and  $d$ , and correspond to Ising-like states), (ii) collective or cooperative ring elementary excitations, (iii) degenerate ground states and spin-glass behavior without disorder, also known as geometric frustration, (iv) correlated motion inside a  $\phi^4$ -type potential, and (v) for increasing temperatures, a type of melting appears that can be described as “correlated melting” in the sense that the “triangle” or

“loop” first melts in the angular coordinate, while the radial coordinate does not melt until much higher temperatures are reached. The elementary excitations are the thermal analog of certain types of squeezed states (where fluctuations strongly affect a coordinate and less the other coordinate). They are also analogs of the “rotational isomers” or “conformations” that are often found in molecules, where three atoms and molecules can cooperatively oscillate back and forth between two degenerate ground states.

At finite temperatures, the three vortices inside the hexagon begin to move and eventually rotate by  $60^\circ$ . This is done cooperatively by the three vortices, and not by one of them individually. They move similarly to the “cooperative rings exchange” mechanism proposed by Feynman for elementary excitations in helium 4. In the case of the second matching field for a kagomé lattice, the elementary excitation of the three interstitial vortices is a  $60^\circ$  rotation, rotating as a cooperative ring. These type of *collective or correlated “cooperative ring exchange”* has also been studied in the context of the quantum Hall effect.

The pinning outside produces a “periodic modulation” of the external boundary, a magnetic trap. The interstitial vortices form a lattice which will slowly melt, through a series of thermal excitations. The first one would be a “one-step click” cooperative ring rotation of  $60^\circ$  (or exchange). Afterwards, several clicks clockwise and counterclockwise, generated by thermal activation, produce angular diffusion.

This type of “controlled melting” of the particles inside a “magnetic trap” could also be visualized with a colloidal suspension surrounded by six pinned (by laser tweezers) charged particles. This type of “vortex-analog” experiment is easier to visualize (optical microscope) than using vortices. Still, Lorentz microscopy techniques would easily monitor such motions.

Decorations experiments could also identify the “blurred” rings or “blurred triangular vertices” due to the thermal excitation of the vortices in the second matching field of the kagomé periodic array of pinning sites.

The melting in circles would be initiated via a sequence of stick-slip discrete motions in “small loops” or “closed strings” formed of concentric 1D Frenkel-Kontorova-type circles. Here the elementary excitations would be “string like” on “closed-loop like.”

## VII. THIRD MATCHING FIELD

In this section we describe the results for a vortex system with  $N_v/N_p^t = 3$ . For this MF the number of interstitial vortices is 2 times the number of triangular pinning sites ( $N_i^t = 2N_p^t$ ) and is 3 times the number of the kagomé pinning sites ( $N_i^k = 3N_p^k$ ). Therefore, it is useful to study the effect of those vortices on the general behavior of the vortex system.

### A. Triangular pinning potential

We study the third MF for a triangular pinning potential in the same way as the previous cases. The trajectories at different temperatures are shown in Fig. 14. In Fig. 14(a) the system is in the liquid phase ( $T > T_p$ ). At  $T < T_p$ ,  $N_p^t$  vortices

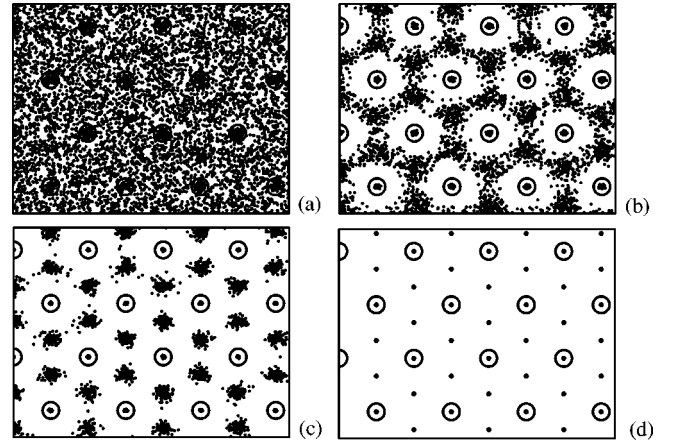


FIG. 14. Vortex trajectories for the third MF with triangular pinning potential. (a)  $T > T_p$ , liquid phase. (b)  $T_p > T > T_i$ , interstitial phase. (c)  $T_i > T$ , solid phase. (d)  $T = 0$ , ground state.

are trapped in the pinning sites, as we can see in Fig. 14(b). The  $N - N_p^t$  interstitial vortices, however, are free to move and they describe the trajectories shown in Fig. 14(b). At a lower temperature  $T_i$ , the interstitial vortices freeze and the vortex trajectories are like Fig. 14(c). The triangular ground state<sup>17</sup> can be observed in Fig. 14(d).

The behavior of the vortex system in this MF reveals that there are two relevant temperatures  $T_p$  and  $T_i$ , the first one which depends on the pinning intensity  $F_p$  and the second almost independent of that parameter.

In Fig. 15(a) we show the pinned fraction  $\chi$  for  $F_p = 5$ . We clearly observe that there are two temperatures separated for this  $F_p$ .

In Fig. 15(b) we plot the  $\langle \Delta r^2(v) \rangle$  for pinned and interstitial vortices. The temperatures  $T_i$  and  $T_p$  are in concordance with the ones defined in Fig. 15(a).

The mean-squared displacements for different time scales are plotted in Fig. 15(c), and they are lower than  $r_p^2$  below  $T_i$ .

In Fig. 15(d) we plot a triangular peak of the structure factor. It has a similar behavior as in the first MF, with a maximum at  $T = 0$ .

### B. Kagomé pinning potential

Finally, we study the third MF with a kagomé pinning potential, and we find a behavior similar to the triangular case. In Figs. 16(a)–16(d) we show vortex positions during the cooling down process. In Fig. 16(a) the system is at a high temperature ( $T > T_p$ ). At  $T < T_p$ ,  $N_p^k$  vortices are in the pinning sites [Fig. 16(b)]. Again, the  $N - N_p^k$  interstitial vortices are free to move. The interstitial vortices freeze at a lower temperature  $T_i$ , and the vortex trajectories are like Fig. 16(c). This behavior is observed also for the fourth MF; the only difference is the number of interstitial vortices.

We find that for the third MF the vortex lattice at  $T = 0$  is always triangular, highly ordered, and the same as obtained for the case with a triangular pinning lattice. The vortices occupy every pinning site, no matter how weak the vortex-pinning interaction is. The vortex lattice is rotated  $30^\circ$  in

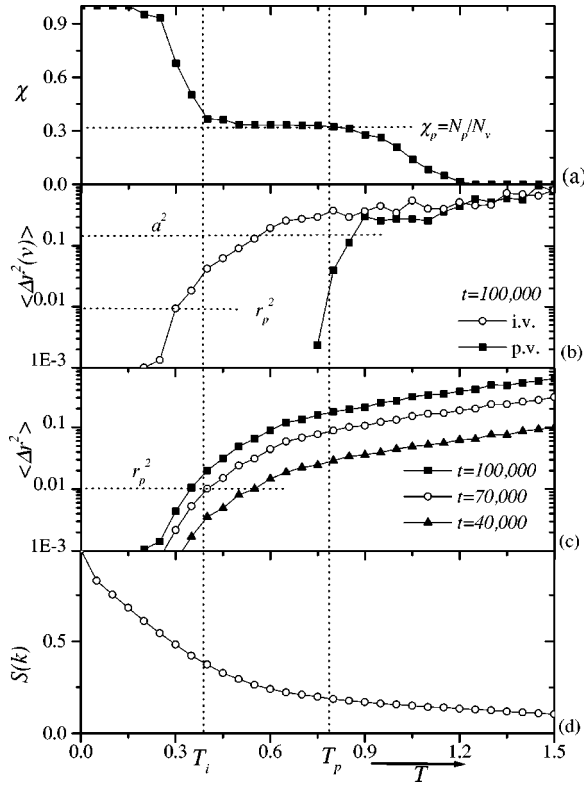


FIG. 15. Third MF of 3072 vortices and  $F_p=5$  for a triangular pinning potential. The following quantities are shown vs temperature: (a) Pinned fractions; (b)  $\langle \Delta r^2(i) \rangle$  of pinned (solid symbols) and interstitial vortices (open symbols), (c) mean-squared displacements at different time scales,  $\langle \Delta r^2 \rangle$ , and (d) the height of the triangular peak of the structure factor.

relation with the pinning array [see Fig. 16(d)]. These structures are stable under small perturbations until the temperature  $T_i$  at which the interstitial vortices start to diffuse.

In Fig. 17 we show the same quantities as in Fig. 15 for a system with the same number of vortices and  $F_p$ . In Fig. 17(a) we show the pinned fraction  $\chi$  for  $F_p=1$  and 5 and we

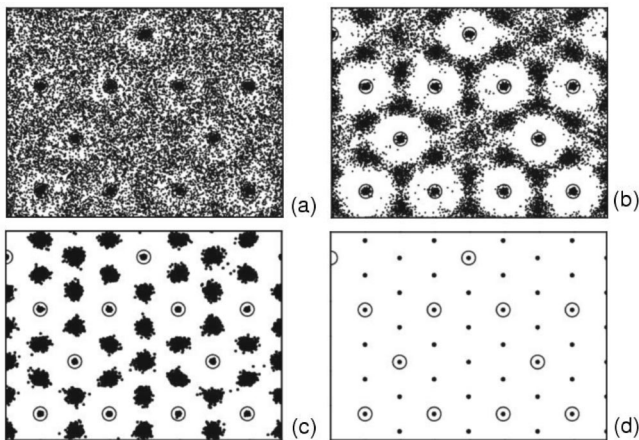


FIG. 16. Vortex trajectories for the third MF. (a)  $T > T_p$ , liquid phase. (b)  $T_p > T > T_i$ , interstitial phase. (c)  $T_i > T$ , solid phase. (d)  $T=0$ , ground state.

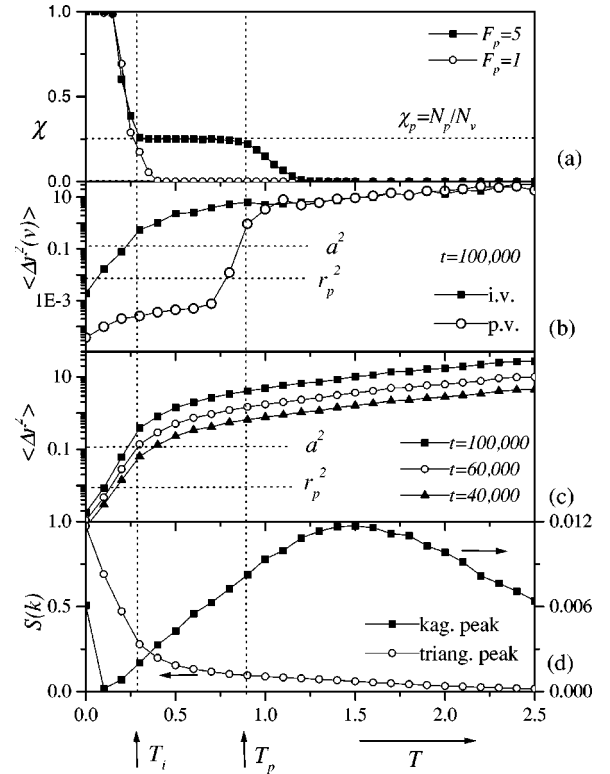


FIG. 17. Third MF of 3072 vortices and  $F_p=5$  for a kagomé pinning potential. Quantities calculated vs temperature: (a) Pinned fraction (we also show  $\chi$  for  $F_p=1$ ), (b)  $\langle \Delta r^2(i) \rangle$  of pinned (open symbols) and interstitial vortices (solid symbols), (c) mean-squared displacements at different time scales,  $\langle \Delta r^2 \rangle$ , and (d) height of two peaks of the structure factor. One corresponding to the triangular lattice of vortices (open symbols) and the other to the kagomé pinning lattice (solid symbols)

can observe that  $T_i$  is the same in both cases but  $T_p$  is moving to a higher temperature as  $F_p$  is increased. We clearly observe that there are two different temperatures for  $F_p=5$ , whereas they coincide for  $F_p=1$ , i.e.,  $T_i=T_p$ .

In Fig. 17(b) we plot the  $\langle \Delta r^2(v) \rangle$  for pinned and interstitial vortices. The temperature  $T_i$  is again in concordance with the  $T_i$  defined in Fig. 17(a), and  $T_p$  coincides with the one defined in  $\chi$  for  $F_p=5$ .

The mean-squared displacement for different time scales is plotted in Fig. 17(c), and shows a change of behavior in  $T_i$ .

Finally, in Fig. 17(d) we plot the two peaks of the structure factor. The behavior of the triangular peak is the same as in the triangular case, with a maximum at  $T=0$ . However, the kagomé peak has a nonzero height at  $T=0$  because the kagomé structure is present still at this temperature. A possible cause of this behavior is the high density of interstitial vortices, which makes possible the contribution of this lattice until  $T=0$ .

## VIII. SUMMARY AND CONCLUSIONS

We have studied the dynamics of a vortex system interacting with a periodic pinning array. We explore the phase-

diagram temperature-pinning intensity for the first three MF's and for the triangular and kagomé pinning geometries. We find several stages of lattice pinning and melting, which depend on the MF studied, i.e., the fraction of interstitial vortices present.

For the first MF we find only one relevant temperature  $T_p$ , below which every vortex is pinned. This behavior was found for the two pinning geometries. The high-temperature region is a liquid phase whereas the low-temperature region is a solid phase.

The second MF with triangular pinning has two characteristic temperatures  $T_p$  and  $T_i$ . The first one is the temperature below which  $N_p^i$  vortices are trapped in the pinning sites, whereas  $T_i$  is the freezing temperature of the  $N_i^i$  interstitial vortices. Besides the solid and liquid phases, there is an intermediate region of temperatures  $T_i < T < T_p$  called the interstitial phase.

For the second MF with kagomé pinning geometry the vortex system has three relevant temperatures  $T_p$ ,  $T_i$ , and  $T_k$ . The first is again the pinning temperature of  $N_p^k$  vortices. The second is the freezing temperature of the interstitial vortices which are trapped inside the kagomé triangles. Finally,  $T_k$  is the freezing temperature of the vortex triangles trapped in the kagomé hexagons. The region  $T_i < T < T_p$  is the interstitial phase, whereas the region  $T_i < T < T_k$  in which the only vortex motion is the rotation of the vortex triangles inside the hexagons is called the kagomé phase.

For the third MF we find two characteristic temperatures  $T_p$  and  $T_i$ , defined as in the second MF with triangular geometry. For both geometries the vortex system has an interstitial phase which has a broader width as higher is the pinning intensity.

The ground state for the first and third MF's is always triangular and highly ordered, and is the same for the two pinning geometries in all the range studied ( $1 < F_p < 5$ ).

The second MF has a partially ordered ground state which

is different for the kagomé and the triangular pinning geometries. The first one is highly degenerated whereas the second has twofold degeneracy.

To reach different ground states after every annealing is standard in glasses, where there is disorder. However, the sample studied here has no disorder (a perfect kagomé array of pins). There is a geometry-induced frustration. Every kagomé hexagon would have two states ( $entropy = k \log 2$ ). Here  $N$  hexagons would have  $2^N$  states, and a very large entropy (of the order of  $N k \log 2$ ). Thus the system has a very large degeneracy and a huge (low- $T$ ) entropy, making it difficult to reach the  $T=0$  ground state.

In conclusion, in most of the cases there are two phase transitions for strong pinning, in which the vortex system pins at a temperature  $T_p$  higher than the freezing temperature of the interstitial vortices,  $T_i$ . This is very different of the well-known case of the submatching fields in periodic potentials, where the pinning temperature is lower than the melting temperature.<sup>23-25</sup>

More interestingly, the kagomé pinning potential shows new low-temperature phases for the second MF, with rotating triangles of vortices and frustration for  $T \rightarrow 0$ .

#### ACKNOWLEDGMENTS

M.F.L. thanks V.I. Marconi, A.B. Kolton, and P.S. Cornaglia for helpful discussions and also acknowledges support from the FOMEC program. We also acknowledge financial support from CONICET, CNEA, ANPCyT, and Fundación Antorchas. F.N. acknowledges the hospitality of the Materials Science Division of Argonne National Laboratory, as well as partial support under DOE Contract No. W-31-109-ENG-38 and from the Center for the Study of Complex Systems at The University of Michigan. This is publication MCTP-01-09 of the Michigan Center for Theoretical Physics.

<sup>1</sup>C. Zeng and V. Elser, Phys. Rev. B **42**, 8436 (1990); P. Chandra and P. Coleman, Phys. Rev. Lett. **66**, 100 (1991); K. Yang, L.K. Warman, and S.M. Girvin, *ibid.* **70**, 2641 (1993); P.W. Leung and V. Elser, Phys. Rev. B **47**, 5459 (1993); P. Chandra, P. Coleman, and I. Ritchey, J. Phys. I **3**, 591 (1993); M.B. Hastings, Phys. Rev. B **63**, 014413 (2001); J.E. Greedan, J. Mater. Chem. **11**, 37 (2001); A.S. Wills, V. Dupuis, E. Vincent, J. Hammann, and R. Calemczuk, Phys. Rev. B **62**, R9264 (2000); P. Sindzinger *et al.*, Phys. Rev. Lett. **84**, 2953 (2000).

<sup>2</sup>V. Elser, Phys. Rev. Lett. **62**, 2405 (1989); D.S. Greywall and P.A. Busch, *ibid.* **62**, 1868 (1989); **65**, 2788 (1990).

<sup>3</sup>A.P. Ramirez, G.P. Espinoza, and A.S. Cooper, Phys. Rev. Lett. **64**, 2070 (1990); C. Broholm, G. Aepli, G.P. Espinosa, and A.S. Cooper, *ibid.* **65**, 3173 (1990); I. Ritchey, P. Coleman, and P. Chandra, Phys. Rev. B **47**, 15 342 (1993).

<sup>4</sup>P. Martinoli, O. Daldini, C. Leemann, and E. Stocker, Solid State Commun. **17**, 205 (1975); P. Martinoli, O. Daldini, C. Leemann, and B. Van den Brandt, Phys. Rev. Lett. **36**, 382 (1976).

<sup>5</sup>B. Pannetier, J. Chaussy, R. Rammal, and J.C. Villegier, Phys.

Rev. Lett. **53**, 1845 (1984); H.D. Hallen, R. Seshadri, A.M. Chang, R.E. Miller, L.N. Pfeiffer, K.W. West, C.A. Murray, and H.F. Hess, *ibid.* **71**, 3007 (1993); K. Runge and B. Pannetier, Europhys. Lett. **24**, 737 (1993).

<sup>6</sup>R.S. Newrock, C.J. Lobb, U. Geigenmuller, and M. Octavio, Solid State Phys. **54**, 263 (2000); *Lectures on Superconducting Networks and Mesoscopic Systems*, edited by C. Giovannella and C. J. Lambert, AIP Conf. Proc. No. **427** (AIP, Woodbury, NY, 1998); J.C. Ciria and C. Giovannella, J. Phys.: Condens. Matter **10**, 1453 (1998); *Macroscopic Quantum Phenomena and Coherence in Superconducting Networks*, edited by C. Giovannella and M. Tinkham (World Scientific, Singapore, 1995); *Proceedings of the ICTP Workshop on Josephson-junction Arrays* [Physica B **222**, 253 (1996)].

<sup>7</sup>C.J. Lobb, D.W. Abraham, and M. Tinkham, Phys. Rev. B **27**, 150 (1983).

<sup>8</sup>See, for example, M.S. Rzchowski, S.P. Benz, M. Tinkham, and C.J. Lobb, Phys. Rev. B **42**, 2041 (1990).

<sup>9</sup>J.I. Martín, M. Vélez, J. Nogués, and Ivan K. Schuller, Phys. Rev.

- Lett. **79**, 1929 (1997); J.I. Martín, M. Vélez, A. Hoffmann, Ivan K. Schuller, and J.L. Vicent, *ibid.* **83**, 1022 (1999).
- <sup>10</sup>D.J. Morgan and J.B. Ketterson, Phys. Rev. Lett. **80**, 3614 (1998); Y. Jaccard, J.I. Martín, M.-C. Cyrille, M. Vélez, J.L. Vicent, and Ivan K. Schuller, Phys. Rev. B **58**, 8232 (1998); T. Puig, E. Rosseel, L. Van Look, M.J. Van Bael, V.V. Moshchalkov, and Y. Bruynseraede, *ibid.* **58**, 5744 (1998); M.J. Van Bael, K. Temst, V.V. Moshchalkov, and Y. Bruynseraede, *ibid.* **59**, 14 674 (1999).
- <sup>11</sup>M. Baert, V.V. Metlushko, R. Jonckheere, V.V. Moshchalkov, and Y. Bruynseraede, Phys. Rev. Lett. **74**, 3269 (1995); K. Harada, O. Kamimura, H. Kasai, T. Matsuda, A. Tonomura, and V.V. Moshchalkov, Science **274**, 1167 (1996); A. Bezryadin, Yu.B. Ovchinnikov, and B. Pannetier, Phys. Rev. B **53**, 8553 (1996).
- <sup>12</sup>T. Matsuda, K. Harada, H. Kasai, O. Kamimura, and A. Tonomura, Science **271**, 1393 (1996).
- <sup>13</sup>J.Y. Lin, M. Gurvitch, S.K. Tolpygo, A. Bourdillon, S.Y. Hou, and J.M. Phillips, Phys. Rev. B **54**, R12 717 (1996); E. Rossel, M. Van Bael, M. Baert, R. Jonckheere, V.V. Moshchalkov, and Y. Bruynseraede, *ibid.* **53**, R2983 (1996); A. Castellanos, R. Wondenweber, G. Ockenfuss, A.v.d. Hart, and K. Keck, Appl. Phys. Lett. **71**, 962 (1997); V.V. Moshchalkov, M. Baert, V.V. Metlushko, E. Rosseel, M.J. van Bael, K. Temst, Y. Bruynseraede, and R. Jonckheere, Phys. Rev. B **57**, 3615 (1998); V. Metlushko, U. Welp, G.W. Crabtree, Zhao, Zhang, S.R.J. Brueck, B. Watkins, L.E. DeLong, B. Ilic, K. Chung, and P.J. Hesketh, *ibid.* **59**, 603 (1999); V. Metlushko, U. Welp, G.W. Crabtree, R. Osgood, S.D. Bader, L.E. DeLong, Zhao Zhang, S.R.J. Brueck, B. Ilic, K. Chung, and P.J. Hesketh, *ibid.* **60**, 12 585 (1999); L.V. Look, L. Van Look, E. Rosseel, M.J. Van Bael, K. Temst, V.V. Moshchalkov, and Y. Bruynseraede, *ibid.* **60**, R6998 (1999).
- <sup>14</sup>S.B. Field, S.S. James, J. Barentine, V. Metlushko, G. Crabtree, H. Shtrikman, B. Ilic, and S.R.J. Brueck, cond-mat/003415 (unpublished).
- <sup>15</sup>Y. Fasano, J.A. Herbsommer, F. de la Cruz, F. Pardo, P.L. Gammel, E. Bucher, and D.J. Bishop, Phys. Rev. B **60**, R15 047 (1999).
- <sup>16</sup>P. Martinoli, Phys. Rev. B **17**, 1175 (1978).
- <sup>17</sup>C. Reichhardt, C.J. Olson, and F. Nori, Phys. Rev. B **57**, 7937 (1998).
- <sup>18</sup>C. Reichhardt, C.J. Olson, J. Groth, S. Field, and F. Nori, Phys. Rev. B **54**, 16 108 (1996).
- <sup>19</sup>W.A.M. Morgado and G. Carneiro, Physica C **238**, 195 (1998).
- <sup>20</sup>V.L. Pokrovskii and A.L. Talanov, Sov. Phys. JETP **51**, 134 (1980).
- <sup>21</sup>P. Martinoli, M. Nsabimana, G.A. Racine, and H. Beck, Helv. Phys. Acta **55**, 655 (1982).
- <sup>22</sup>C. Reichhardt, C.J. Olson, and F. Nori, Phys. Rev. Lett. **78**, 2648 (1997); Phys. Rev. B **58**, 6534 (1998).
- <sup>23</sup>D. R. Nelson, in *Phase Transitions and Critical Phenomena*, edited by C. Domb and J. L. Lebowitz (Academic, New York, 1983), Vol. 7.
- <sup>24</sup>M. Franz and S. Teitel, Phys. Rev. Lett. **73**, 480 (1994); Phys. Rev. B **51**, 6551 (1995).
- <sup>25</sup>S. Hattel and J.M. Wheatley, Phys. Rev. B **51**, 11 951 (1995).
- <sup>26</sup>C. Reichhardt and F. Nori, Phys. Rev. Lett. **82**, 414 (1999).
- <sup>27</sup>V.I. Marconi and D. Domínguez, Phys. Rev. Lett. **82**, 4922 (1999).
- <sup>28</sup>G. Carneiro, J. Low Temp. Phys. **177**, 1323 (1999).
- <sup>29</sup>C. Reichhardt and G. Zimanyi, Phys. Rev. B **61**, 14 354 (2000).
- <sup>30</sup>V.I. Marconi, S. Candia, P. Balenzuela, H. Pastoriza, D. Domínguez, and P. Martinoli, Phys. Rev. B **62**, 4096 (2000); V.I. Marconi and D. Domínguez, *ibid.* **63**, 174509 (2001).
- <sup>31</sup>A.E. Koshelev and V.M. Vinokur, Phys. Rev. Lett. **73**, 3580 (1994).
- <sup>32</sup>See, for instance, the reviews by B. Pannetier, J. Chaussy, and R. Rammal, Jpn. J. Appl. Phys., Part 1 **26**, 1994 (1987); P. Martinoli, *ibid.* **26**, 1989 (1987); C.J. Lobb, Physica B **126**, 319 (1984); and the many articles in the issue on “Coherence in superconducting networks,” edited by J. E. Mooij and G. B. J. Schön [Physica B **152**, 1 (1988)].
- <sup>33</sup>Y.-L. Lin and F. Nori, Phys. Rev. B **50**, 15 953 (1994); and (unpublished).
- <sup>34</sup>M.J. Higgins, Y. Xiao, S. Bhattacharya, P.M. Chaikin, S. Sethuraman, R. Bojko, and D. Spencer, Phys. Rev. B **61**, R894 (2000); Y. Xiao *et al.* (unpublished).
- <sup>35</sup>J.B. Nielsen, T. Sondergaard, S.E. Barkou, A. Bjarklev, and J. Broeng, IEEE Photonics Technol. Lett. **12**, 630 (2000).